Magneto-elastic phase transitions in one-dimensional systems

2009 J. Phys.: Condens. Matter 21 046001

(http://iopscience.iop.org/0953-8984/21/4/046001)

J. Phys.: Condens. Matter **21** (2009) 046001 (8pp) doi:10.1088/0953-8984/21/4/046001

Magneto-elastic phase transitions in one-dimensional systems

J R Suárez[1], E Vallejo[1], O Navarro[1] and M Avignon[2]

[1] Instituto de Investigaciones en Materiales, Universidad Nacional Autónoma de México, Apartado Postal 70-360, 04510 México DF, Mexico
[2] Institut Néel, Center National de la Recherche Scientifique (CNRS) and Université Joseph Fourier, BP 166, 38042 Grenoble Cedex 9, France

E-mail: jrsuarez@iim.unam.mx

Received 2 October 2008, in final form 18 November 2008
Published 15 December 2008
Online at stacks.iop.org/JPhysCM/21/046001

Abstract
The magneto-elastic phase diagram in one-dimensional systems relating to the interplay between magnetism and lattice distortion is studied in a double-exchange and super-exchange model considering classical localized spins and the limit of large Hund's coupling. At low super-exchange interaction energy, a phase transition occurs between electron-full ferromagnetic distorted and electron-empty antiferromagnetic undistorted phases via phase separation. In this case, all electrons and lattice distortions are found within the ferromagnetic domain. For higher super-exchange interaction energy, phase separations consisting of two- or three-site distorted independent magnetic polarons separated by electron-empty undistorted antiferromagnetic links are obtained. In this regime, each polaron contains an electron, leading to a Wigner crystallization. The lattice distortion and charge distribution inside the polarons are also calculated.

1. Introduction

The physics of transition-metal oxides has revealed a variety of phenomena in the last few decades [1, 2]. Among those phenomena, colossal magnetoresistance (CMR) has attracted great interest, not only as a challenging subject of fundamental science but also as an important phenomenon for potential spintronic applications. Typically, the materials that present this phenomenon have a perovskite type lattice structure and display a broad spectrum of physical properties depending on the filling, temperature and other parameters. Theoretical studies are widely based on the so-called double-exchange (DE) model introduced by Zener [3, 4] to explain the ferromagnetism of manganites. The origin of the DE mechanism lies in the intra-atomic Hund's spin coupling J_H between itinerant and localized electrons. This mechanism has been widely used in the context of manganites [3–7]. The key point is that this coupling implies that the hopping depends on the configuration of the neighbor spins and explains how carriers improve their kinetic energy by forcing the localized spins to become ferromagnetically ordered. This ferromagnetic (F) tendency is expected to be frustrated by antiferromagnetic (AF) super-exchange (SE) interactions between localized spins $\vec{S}_i$ as first discussed by de Gennes [8] who conjectured the existence of canted states. Since then, it has become clear that microstructured spin configurations exist rather than macroscopic canted states resulting from such competition. Naturally, the strength of the magnetic interactions depends significantly on the conduction band filling. At low electron density, ferromagnetic polarons have been found for localized $S = 1/2$ quantum spins [9, 10]. 'Island' phases, periodic arrangements of F polarons coupled antiferromagnetically, have been clearly identified at commensurate fillings both for quantum spins in one dimension [11, 12] and for classical spins in one (1D) [13] and two dimensions (2D) [14]. Phase separation between hole-undoped antiferromagnetic and hole-rich ferromagnetic domains has been obtained in the ferromagnetic Kondo model [15, 16]. Phase separation and small ferromagnetic polarons have also been identified for localized $S = 3/2$ quantum spins [17]. Recently, a unifying picture in 1D for classical local spins has shown the existence of two-and three-site ferromagnetic polarons separated by AF links over the whole range of electron density [18, 19]. As a result of the spin dependent hopping, carriers are localized in the ferromagnetic bonds, giving rise to bond ordered states for commensurate fillings. In turn, this will induce significant lattice distortions in systems in which the electrons interact

with the lattice by affecting the hopping amplitude as in the Su–Schrieffer–Heeger (SSH) model [20, 21]. This point implies an important connection between the magnetic structure and lattice distortions. Up to now, in spite of its simplicity, this magneto-elastic effect has attracted very little attention, although it might be particularly important in one-dimensional and quasi-one-dimensional materials, such as halogen bridged metal chains, conjugated polymers, ladders and a variety of charge-transfer salts [22]. Recently, Vallejo *et al* [23–25] have shown that three-leg ladders in the oxyborate system Fe_3BO_5 may provide evidence for the interplay between the magnetic structure and the observed structural and charge ordering transition, such that long and short bonds on the rungs alternate along the ladder axis [26]. For Fe ludwigite, x-ray diffraction studies show contraction of the rungs [27].

The main goal of this work is to study the interplay between magnetic interactions and lattice distortion in one-dimensional systems. We consider the SSH model for the electron–lattice coupling together with the double-exchange and super-exchange model. It is important to note the difference from the electron–lattice coupling usually taken for manganites, which arises from the Jahn–Teller splitting of the doubly degenerate levels [28, 29]. As in [18] we will determine the phase diagram as a function of the band filling and the super-exchange interaction energy, and we will examine the effect of including coupling with the lattice.

2. The model and basic trends

We consider the DE–SE Hamiltonian for describing the localized and itinerant electrons:

$$H_{\mathrm{DE-SE}} = -\sum_{i,\sigma} t_{i,i+1}(c^{\dagger}_{i,\sigma}c_{i+1,\sigma} + \mathrm{h.c.}) - J_{\mathrm{H}}\sum_{i}\vec{S}_i\cdot\vec{\sigma}_i + J\sum_{i}\vec{S}_i\cdot\vec{S}_{i+1}, \quad (1)$$

where $c^{\dagger}_{i\sigma}$ ($c_{i\sigma}$) are the fermion creation (annihilation) operators for conduction electrons at site i and spin σ, $t_{i,i+1} = t$ is the nearest-neighbor (n.n.) hopping parameter and J_{H} is Hund's intra-atomic exchange coupling between the spin of conduction $\vec{\sigma}_i$ and localized $\vec{S}_i$ spins. The first two terms represent the DE contribution favoring F ordering of local spins whose robustness depends on the number of conduction electrons per site x. The last term is a SE coupling between n.n. localized spins $\vec{S}_i$, J being an AF interaction energy which stabilizes an AF phase for $x = 0$ and competes with DE for intermediate fillings.

Finally, we introduce the effect of bond deformation on the itinerant electrons. In the SSH model, the complicated inter-atomic potential is represented using the electron–lattice coupling constant $g_t \simeq \partial t/\partial y$ ($g_t < 0$) which describes the change of the hopping amplitude under a small change of the n.n. bond length y:

$$H_{\mathrm{e-l}} = g_t\sum_{i,\sigma} y_{i,i+1}(c^{\dagger}_{i\sigma}c_{i+1,\sigma} + \mathrm{h.c.}) + \frac{K_t}{2}\sum_{i} y^2_{i,i+1}, \quad (2)$$

where $y_{i,i+1}$ is the change of the $i, i+1$ lattice distance. It is important to mention that the original equilibrium lattice spacing a_0 (and so also t) in the absence of $H_{\mathrm{e-l}}$ results from the bonding produced by all other electrons in the system except the itinerant ones that we are considering in (1). The elastic constant K_t refers to this equilibrium lattice. Conduction electrons give an additional bonding which manifests itself in a contraction of the lattice $\Delta L = \sum_i^{N-1} y_{i,i+1} \leqslant 0$.

The electron–lattice part may be written in the following standard form, introducing the dimensionless parameters for the deformation $\delta_{i,i+1} = g_t y_{i,i+1}/t$ and the usual coupling constant $\lambda = 2g_t^2/\pi t K_t$:

$$H_{\mathrm{e-l}} = -t\sum_{i,\sigma}\delta_{i,i+1}(c^{\dagger}_{i,\sigma}c_{i+1,\sigma} + \mathrm{h.c.}) + \frac{t}{\pi\lambda}\sum_{i}\delta^2_{i,i+1}. \quad (3)$$

The hopping term changes as $t_{i,i+1} = t(1+\delta_{i,i+1})$ with $|\delta_{i,i+1}| \ll 1$. The total Hamiltonian is

$$H = -t\sum_{i,\sigma}\left(1+\delta_{i,i+1}\right)(c^{\dagger}_{i\sigma}c_{i+1,\sigma} + \mathrm{h.c.}) - J_{\mathrm{H}}\sum_{i}\vec{S}_i\cdot\vec{\sigma}_i + J\sum_{i}\vec{S}_i\cdot\vec{S}_{i+1} + \frac{t}{\pi\lambda}\sum_{i}\delta^2_{i,i+1}. \quad (4)$$

The DE simplifies in the strong coupling limit [7, 30] $J_{\mathrm{H}} \to \infty$, a limit commonly called the DE model. We will consider the local spins as classical $\vec{S}_i \to \infty$, a reasonable approximation in many cases in view of the similarity of the known results [11, 12, 15, 16]. So, the DE part takes the well-known form $-\sum_i t_{i,i+1}\cos(\frac{\theta_{i,i+1}}{2})(c^{\dagger}_i c_{i+1} + \mathrm{h.c.})$ and the complete Hamiltonian is given by

$$H = -t\sum_{i}\left(1+\delta_{i,i+1}\right)\cos\left(\frac{\theta_{i,i+1}}{2}\right)(c^{\dagger}_i c_{i+1} + \mathrm{h.c.}) + JS^2\sum_{i}\cos\left(\theta_{i,i+1}\right) + B\sum_{i}\delta^2_{i,i+1}, \quad (5)$$

where $B/t = 1/\pi\lambda$. The itinerant electrons being now either parallel or antiparallel to the local spins are thus *spinless*. $\theta_{i,i+1}$ ($0 \leqslant \theta_{i,i+1} \leqslant \pi$) is the relative angle between the classical localized spins at sites i and $i+1$ which are specified by their polar angles ϕ_i, φ_i defined with respect to a z-axis taken as the spin quantization axis of the itinerant electrons. In the case of quantum spins we should consider that the hopping amplitude depends on the n.n. spin configuration through the spin–spin correlation.

The correlation between the magnetic structure and lattice deformations is transparent in (5); due to the dependence of the hopping amplitude on the spin configuration, the contribution of the itinerant electrons to the metallic bonding varies with the magnetic state and so will the resulting lattice spacing. In a single bond with one electron, if the local spins are ferromagnetic, the bonding is that of a simple diatomic molecule with hopping t; the bonding energy is just $-t(1+\delta_0)$ resulting in $\delta_0 = t/2B$ and bond contraction. In contrast, if the configuration is AF ($t_e = 0$), the electron becomes localized and does not produce either additional bonding ($\delta = 0$) or length change.

In the thermodynamic limit within an homogeneous F phase ($\delta_{i,i+1} = \delta_u, \theta_{i,i+1} = 0$) the energy is written as

$$E = -\frac{2t(1+\delta_u)}{\pi}\sin\pi x + B\delta_u^2 + JS^2, \quad (6)$$

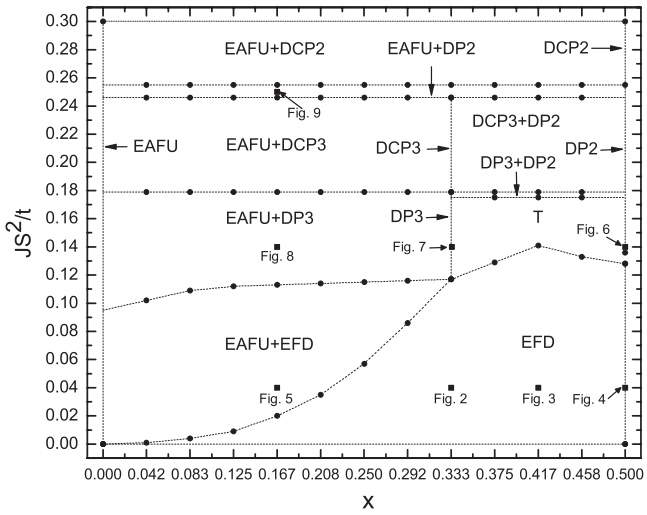

Figure 1. Magneto-elastic phase diagram as a function of the SE interaction energy JS^2/t and the conduction electron density x, for a typical value of the elastic energy $B/t = 30$. The dotted line in this diagram is a guide to the eyes. The different phases are described in the text.

which gives $\delta_u = (t/\pi B)\sin\pi x = \lambda \sin\pi x$; $\delta_u > 0$ means a contraction of the lattice. How the bond length is affected results from the electron–lattice coupling parameter g_t, $y_{i,i+1} = (t/g_t)\delta_{i,i+1}$. The cohesive energy E as a function of the band filling is similar to the Friedel model which gives a qualitatively correct prediction of the trends in transition metals (see for example [31]). In general, in addition to the homogeneous δ_u, a staggered Peierls distortion δ_s is also expected in such one-dimensional systems.

The same effect will occur in other homogeneous phases, like a paramagnetic phase for example. In that case, the effective hopping results from averaging over all the possible values of $\theta_{i,i+1}$, $t_e = t\langle\cos(\frac{\theta_{i,i+1}}{2})\rangle = \frac{2}{3}t$ and the lattice contraction will be smaller than in the ferromagnetic case. On the other hand, in an AF phase the lattice spacing remains unchanged: $a = a_0$. Clearly, through lattice distortions clear distinctions can be made between F and AF regions, particularly interesting when there exist magnetically microstructured phases, as are found resulting from the competition between DE and SE [18, 19, 23].

This magneto-elastic effect also exists, although it is smaller, in the local quantum $S = 1/2$ spin case. For large $J_H > 0$, the Hund term stabilizes a $S = 1$ triplet state when a conduction electron is on that site, so hopping takes place within this state. In a F state, all local electrons have, let us say, $m_S = 1/2$, so an electron hops from a site with $m_S = +1$ to a site where it will produce also $m_S = +1$ and the hopping remains equal to t. In an AF bond the hopping is between a site with $m_S = +1$ and a site with $m_S = 0$, and is equal to $t/\sqrt{2}$, smaller than for a F bond. Therefore, the classical spin limit enhances the lattice change between F and AF bonds.

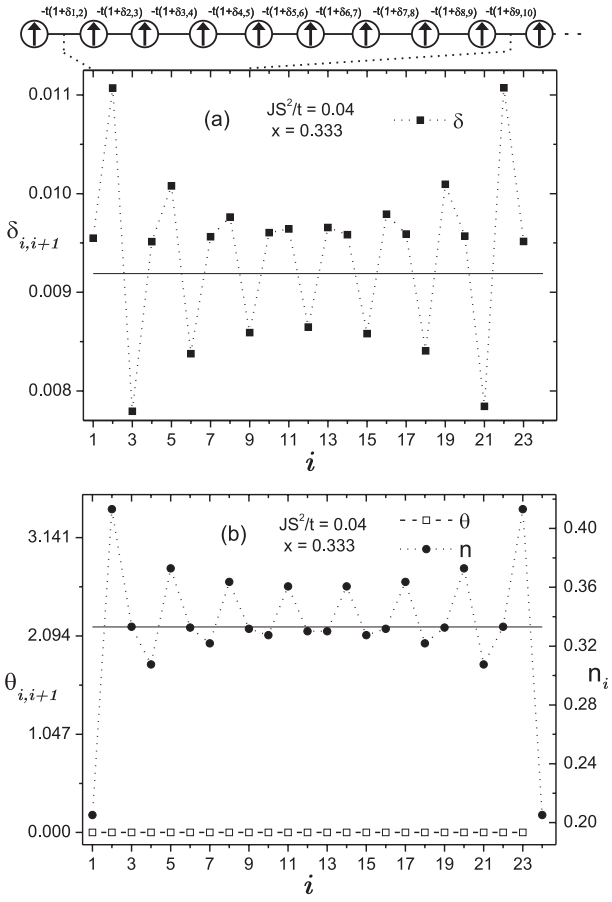

Figure 2. EFD phase for eight electrons ($x = 1/3$) and $JS^2/t = 0.04$ showing: (a) ($\delta_{i,i+1}$) and (b) angles ($\theta_{i,i+1}$) and charge distribution (n_i). Solid lines represent the thermodynamic limit. A partial spin configuration snapshot is also shown.

3. Numerical results and discussion

The phase diagram for the model given by (5) is obtained as a function of the conduction electron density x ($0 \leqslant x \leqslant 0.5$ because of hole–electron symmetry) and the SE interaction energy J. $T = 0$ K and open boundary conditions on a linear chain of $N = 24$ sites were used. $N-1$ angles $\theta_{i,i+1}$ and $N-1$ values of $\delta_{i,i+1}$ had to be optimized. For this goal, classical Monte Carlo simulations are used, energies being obtained by numerical diagonalization of Hamiltonian (5). In general, this allows a simple description of the phases in terms of a small number of variables, making possible an analytical study which confirms the phase boundaries obtained numerically. The Z-eigenvalues of the Hamiltonian (5) can be calculated using the following determinant:

$$\det\begin{pmatrix} -Z & h_{1,2} & 0 & \cdots & 0 \\ h_{2,1} & -Z & h_{2,3} & \cdots & 0 \\ 0 & h_{3,2} & -Z & \ddots & \\ \vdots & \vdots & \ddots & \ddots & h_{N-1,N} \\ 0 & 0 & & h_{N,N-1} & -Z \end{pmatrix} = 0, \qquad (7)$$

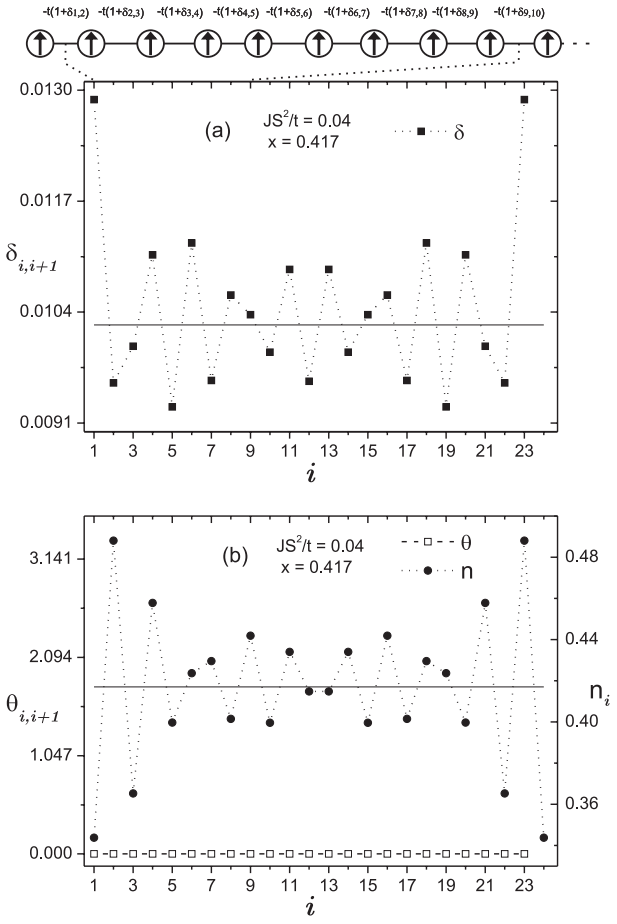

Figure 3. EFD phase for ten electrons ($x = 0.417$) and $JS^2/t = 0.04$, showing the same as figure 2.

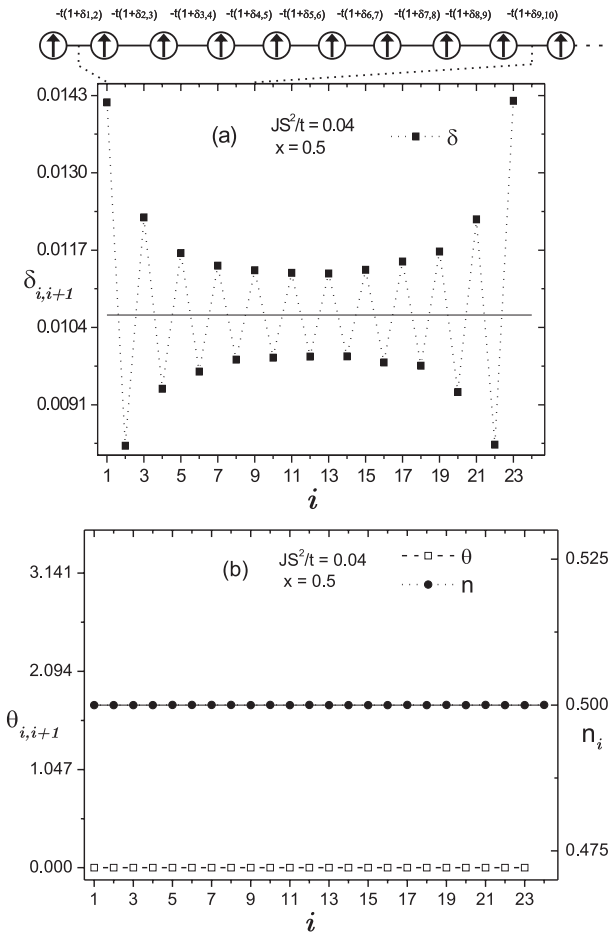

Figure 4. EFD phase for twelve electrons ($x = 0.5$) and $JS^2/t = 0.04$, showing the same as figure 2.

where $h_{i+1,i} = h_{i,i+1} = -t(1 + \delta_{i,i+1}) \cos(\frac{\theta_{i,i+1}}{2})$. The total energy U can be obtained as

$$U = E_{\text{Kin}} + E_{\text{Mag}} + E_{\text{Elas}}, \tag{8}$$

where

$$E_{\text{Kin}} = \sum_{i=1}^{\epsilon_{\text{F}}} Z_i,$$

$$E_{\text{Mag}} = JS^2 \sum_{i=1}^{N-1} \cos\left(\theta_{i,i+1}\right)$$

and

$$E_{\text{Elas}} = B \sum_{i=1}^{N-1} \delta_{i,i+1}^2.$$

Here ϵ_{F} is Fermi's energy.

In figure 1 we present results for $B/t = 30$ which correspond to the very weak coupling limit $\lambda \approx 0.01$, to guarantee small $\delta_{i,i+1}$ and also small displacements of all the atoms. However, systems in which the bonding is more important, with larger λ, could also be envisaged.

At first sight, the results look like the magnetic-only phase diagram without lattice distortion, $\delta_{i,i+1} = 0$ ($B/t \to \infty$), studied recently [18, 19]. The microstructured magnetic phases involved are basically the same, but with inhomogeneous lattice distortions. As expected, the AF links are always undistorted.

First, there is the region where the ground state is F, as shown in figures 2–4 for different electronic densities $x = 1/3$, $x = 5/12$, $x = 1/2$ and $JS^2/t = 0.04$. In these figures we show angles $\theta_{i,i+1}$, lattice distortion $\delta_{i,i+1}$, charge distribution n_i and a partial spin configuration snapshot through the system. Solid lines represent the homogeneous thermodynamic limit values δ_u and $n_i = x$. The oscillating departures from these values are due to finite size effects resulting from open boundary conditions. For larger system sizes we recovered the homogeneous δ_u in the center of the finite system. As mentioned above, a Peierls type distortion δ_s should also be observed; however it is negligibly small for the very weak coupling situation that we present here. At lower densities, between the AF phase at $x = 0$ and the F phase, we find a phase separation consisting of a large distorted F region containing all the electrons (EFD) within an AF undistorted phase without electrons (EAFU) as shown in figure 5. In this figure, solid lines also represent the thermodynamic limit δ_u for the electron density inside EFD ($x = 2/9$ in this case) and $n_i = x$. The optimized solution proposed gives $\theta_{i,i+1} = 0$ and π exactly for the ferromagnetic and antiferromagnetic domains respectively. In this case, the open boundary conditions apply due to the

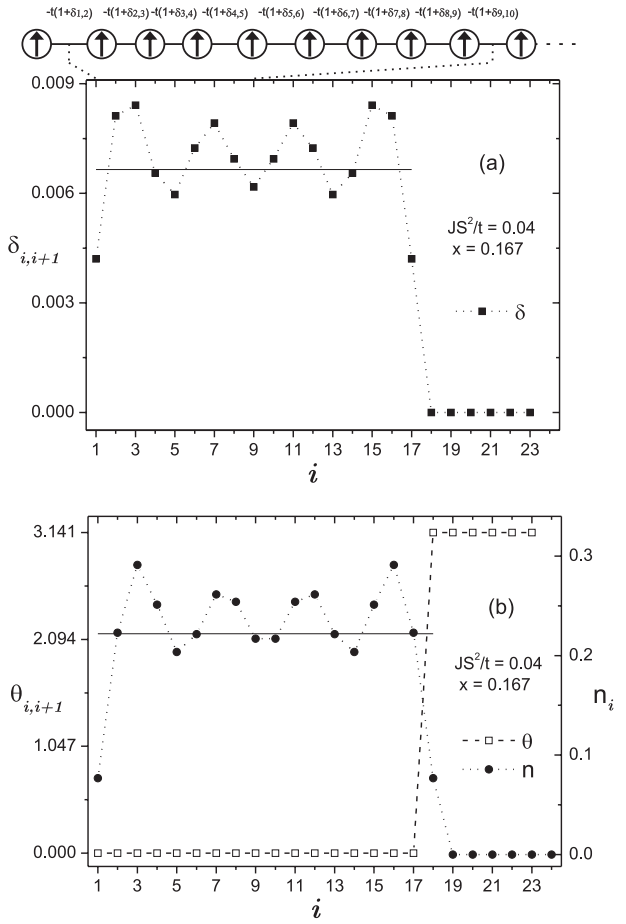

Figure 5. EAFU + EFD phase separation for four electrons ($x = 0.167$) and $JS^2/t = 0.04$ showing: (a) $\delta_{i,i+1}$ and (b) angles and charge distribution. A partial spin configuration snapshot is also shown.

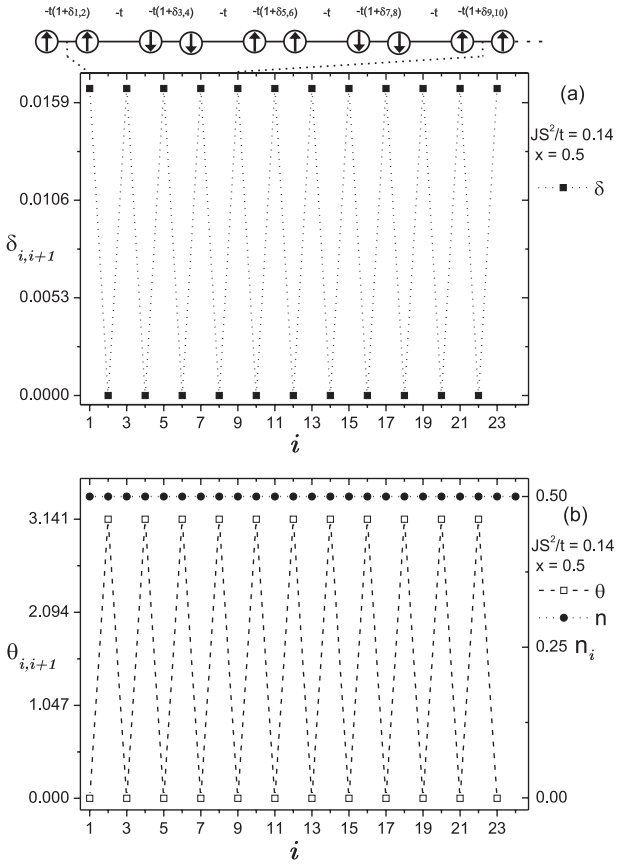

Figure 6. DP2 phase at $x = 0.5$ showing (a) $\delta_{i,i+1}$ and (b) angles and charge distribution. The partial spin configuration snapshot is also shown.

AF links, explaining the inhomogeneous distribution. In this regime of low J, a phase separation (F + AF; for the magnetic case only) has been reported in two dimensions [32], in one dimension using classical localized spins and $J_H = 8$ [33] and in the one-dimensional ferromagnetic Kondo model [34]. We should mention that, in this limit, our results differ from those of Koshibae *et al* [13] within the 'spin-induced Peierls instability' mechanism.

When JS^2/t increases ($JS^2/t \gtrsim 0.12$), small independent magnetic polarons appear; in these cases an analytical solution can be obtained since the 24×24 matrix is indeed a 3×3 block matrix. So, the analytical solution can be easily achieved by solving these 3×3 matrices [35].

For the commensurate filling $x = 1/2$, above the EFD phase, with increasing JS^2/t, we recover the P2 phase ($\theta_i = 0$ inside the polaron) and then the CP2 phase (canted P2, $\theta_i = \theta$) consisting of two-site polarons coupled antiferromagnetically but distorted. Each polaron traps one electron. These phases are labeled DP2 and DCP2; DP2 (with $\delta_0 = t/2B$) is shown in figure 6. In the DCP2 phase the two spins are canted and accordingly δ_i is smaller than in DP2. Similarly the DP3 phase with three-site distorted polarons coupled antiferromagnetically ($\theta_1 = \theta_2 = 0, \delta_1 = \delta_2 = \delta_p$) is obtained for $x = 1/3$ (figure 7) which transforms into DCP3 (distorted canted P3) at larger JS^2/t. One important effect of the electron–lattice coupling is that the continuous degeneracy of the angles θ_1 and θ_2 previously found for the CP3 phase [18, 19] is now broken [36]. The three-site polarons with one electron are independent and their energy is

$$E/t = -\sqrt{(1+\delta_1)^2 \cos^2\frac{\theta_1}{2} + (1+\delta_2)^2 \cos^2\frac{\theta_2}{2}} + \frac{JS^2}{t}(\cos\theta_1 + \cos\theta_2) + \frac{B}{t}(\delta_1^2 + \delta_2^2). \quad (9)$$

In the absence of lattice distortion we obtain the minimum energy state for $\cos\theta_1 + \cos\theta_2 = \frac{1}{8(JS^2/t)^2} - 2$. However, with lattice distortion we get the following succession of phases (see figure 1). First we find the DP3 phase ($\theta_1 = \theta_2 = 0$, $\delta_1 = \delta_2 = \delta_p = t/2\sqrt{2}B$ inside each polaron); see figure 7. DP3 transforms into a partially canted DCP3 phase in which one bond only is canted. In this phase one angle remains zero and the other one is finite $\theta_2 = \theta$ until this angle θ_2 reaches π (we have then DP2 + one AF bond). Finally the other bond becomes canted ($\theta_1 = \theta$, $\theta_2 = \pi$; indeed DCP2 + one AF bond) $\uparrow\uparrow\uparrow$ ($P3$) $\longrightarrow\uparrow\uparrow\nearrow\longrightarrow\uparrow\uparrow\downarrow\longrightarrow\nwarrow\nearrow\swarrow$. DP3 becomes DCP3 for intermediate SE interaction energy $0.179 \lesssim JS^2/t \lesssim 0.245$. DP2 is stable in a small range above $JS^2/t \simeq 0.245$. DP2 becomes DCP2 for $JS^2/t \gtrsim 0.254$. In the region above EFD and EAFU + EFD phases and for

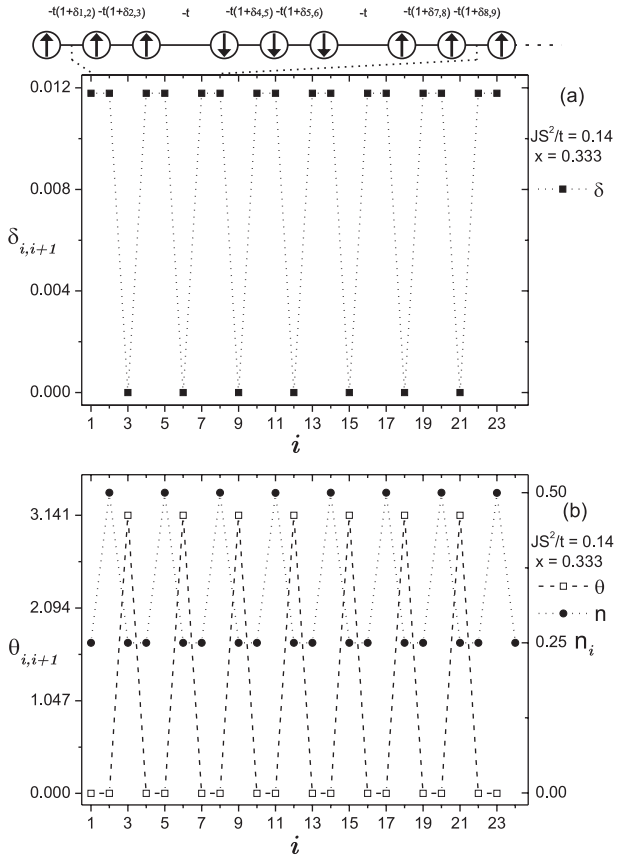

Figure 7. DP3 phase at $x = 1/3$, showing the same in figure 6.

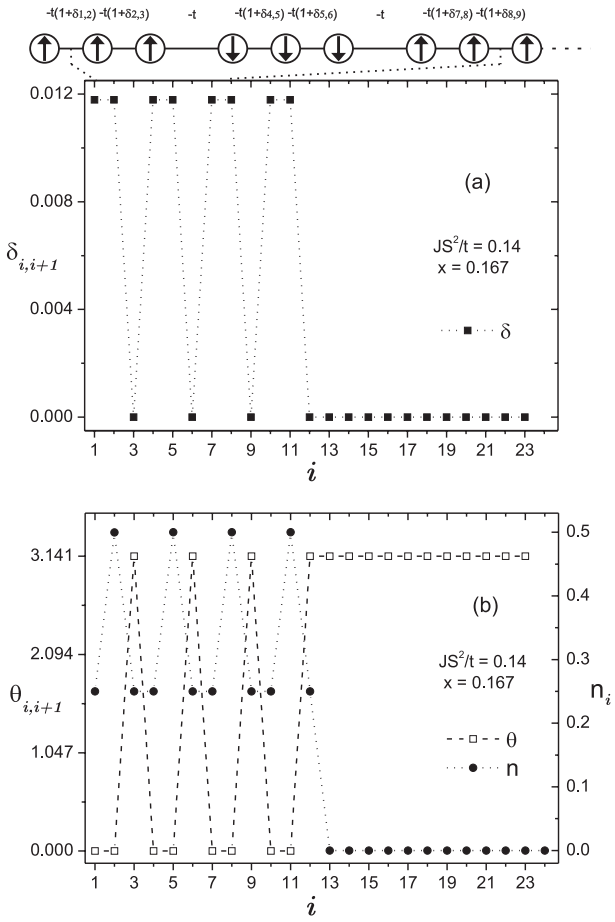

Figure 8. EAFU + DP3 phase for four electrons ($x = 0.167$) and $JS^2/t = 0.14$, showing the same as figure 6.

$JS^2/t \lesssim 0.245$, we find different phases for $x < 1/3$ and $1/3 < x < 1/2$. For $0 < x \leqslant 1/3$ and $JS^2/t \lesssim 0.179$, we can observe EAFU + DP3 phase separation (figure 8) consisting of DP3 polarons immersed in an AF background. This transforms into EAFU + DCP3 for $JS^2/t \gtrsim 0.179$ as DP3 becomes DCP3. EAFU + DP3 and EAFU + DCP3 phase separations are degenerate with phases where the polarons can be ordered or not, while keeping the number of F and AF bonds fixed; phases obtained within the 'spin-induced Peierls instability' [13] belong to this class. For $x > 1/3$, the T phase is a more general complex distorted phase found by the Monte Carlo method and can be polaronic like or not. The expected DCP3 + DP2 phase separation is obtained for $0.179 \lesssim JS^2/t \lesssim 0.245$. A phase DP3 + DP2 is found in a very narrow region between T and DCP3 + DP2.

For strong SE interactions $JS^2/t \gtrsim 0.245$, we obtain EAFU + DP2 (only in the narrow range corresponding to the stability of DP2 for $x = 1/3$) and EAFU + DCP2 over the whole range of electronic concentration. As we have seen, these two-site polaron states are stabilized by the coupling with the lattice. In the absence of distortions they belong to all the possible degenerate states. Figure 9 shows the EAFU +DP2 phase separation for the case of four electrons and $JS^2/t = 0.25$. Two-and three-site polarons always show bond contractions $y_{i,i+1}$, therefore producing small magneto-elastic polarons. The overall lattice contraction $\Delta L = \sum_i^{N-1} y_{i,i+1} = (t/g_t) \sum_i^{N-1} \delta_{i,i+1}$ for the different phases is shown in figure 10 in units of t/g_t. In figure 11, we present the total energy U/Nt as a function of the electronic conduction density for different values of the super-exchange interaction energy. As expected, ΔL and U/Nt varies linearly with x within phase separated regions as indicated by the straight lines in these figures. In DP2, DCP2, DP3 and DCP3 phases each polaron traps a single electron, so forming a Wigner crystallization. As for the EAFU + DP3 and EAFU + DCP3 phase separations, all the phases involving DP2, DCP2, DP3 and DCP3 polarons are degenerate with respect to their position, ordered or not, while keeping the number of F and AF bonds fixed. The former degeneracy unifies ideas like phase separation and individual polarons and gives a natural response to the instability at the Fermi energy and to an infinite compressibility as well.

4. Summary

We have studied the rich phase diagram resulting from the interplay between magnetic interactions and lattice distortion within an exchange model in one-dimensional systems using large Hund's coupling and classical localized spins. Basically, microstructured phases with small ferromagnetic polarons result from the double-exchange and super-exchange interaction. Our results for low SE interaction energy show phase separation between ferromagnetic and antiferromagnetic

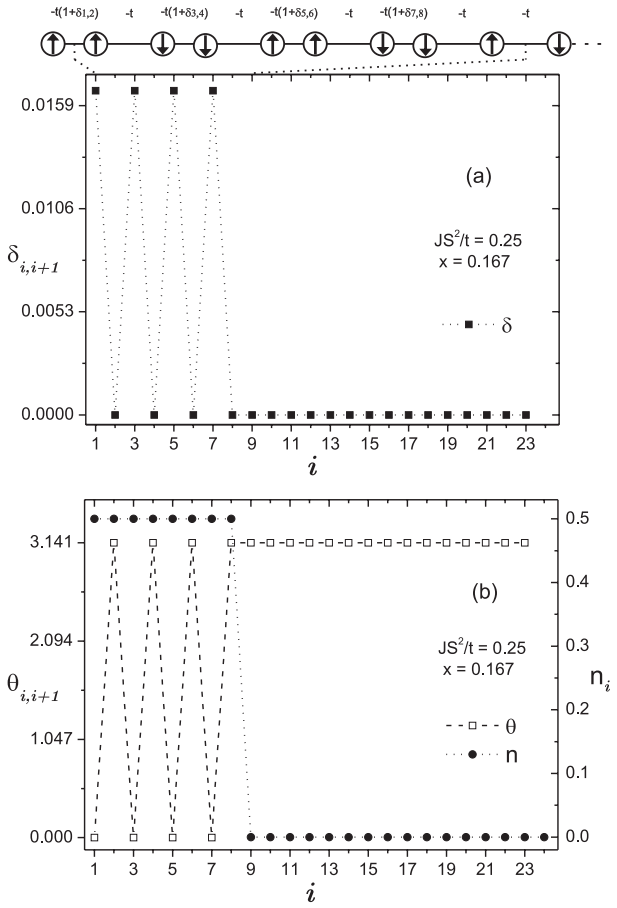

Figure 9. EAFU + DP2 phase for four electrons ($x = 0.167$) and $JS^2/t = 0.25$, showing the same as figure 6.

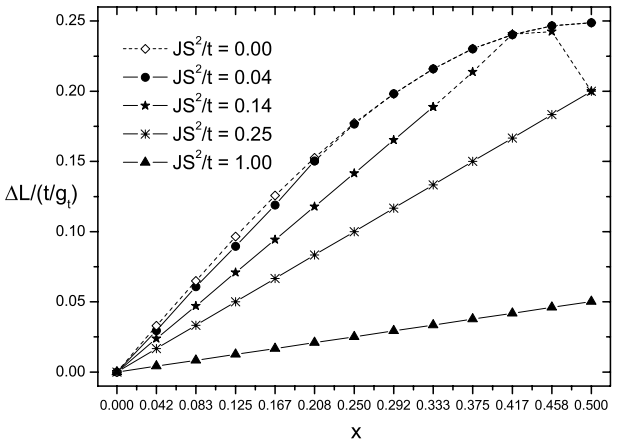

Figure 10. Lattice contraction ΔL in units of t/g_t as a function of the electronic conduction density x for different values of the super-exchange interaction energy JS^2/t. Dashed lines are guides to the eyes.

phases. In this case, the ferromagnetic domain contains all the electrons and a lattice contraction occurs only within this domain. For larger SE interaction energy, we found phase separations involving small two-and three-site distorted polarons, in which a Wigner crystallization can be identified. The important magneto-elastic effect obtained here leads to

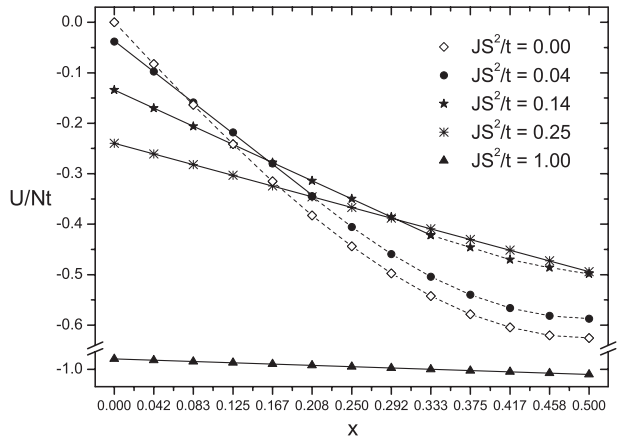

Figure 11. Total energy U/Nt as a function of the electronic conduction density x for typical values of the super-exchange interaction energy JS^2/t. Solid lines represent phase separation energies and dashed lines are guides to the eyes.

local bond contractions that consequently change the lattice parameters which should be observable. We expect this effect to occur in low-dimensional systems in which magnetic ions coupled via a double-exchange type interaction are present, for example molecular magnets, halogen bridged metal chains and charge-transfer salts. Ladders in the ludwigite family seem to be good candidates also.

Acknowledgments

We wish to acknowledge partial support from CONACyT Grant-57929 and PAPIIT-IN108907 from UNAM. EV acknowledges DGAPA-UNAM for financial support.

References

[1] Kaplan T A and Mahanti S D 1999 *Physics of Manganites* (New York: Kluwer Academic/Plenum)
[2] Tokura Y 2000 *Colossal Magnetoresistive Oxides* (*Advances in Condensed Matter Science* vol 2) (Amsterdam: Gordon and Breach)
[3] Zener C 1951 *Phys. Rev.* **82** 403
[4] Zener C 1951 *Phys. Rev.* **81** 440
[5] Jonker G H and Van Santen J H 1950 *Physica* **16** 337
[6] Jonker G H and Van Santen J H 1950 *Physica* **16** 599
[7] Anderson P W and Hasegawa H 1955 *Phys. Rev.* **100** 675
[8] de Gennes P G 1960 *Phys. Rev.* **118** 141
[9] Batista C D, Eroles J, Avignon M and Alascio B 1998 *Phys. Rev.* B **58** R14689
[10] Batista C D, Eroles J, Avignon M and Alascio B 2000 *Phys. Rev.* B **62** 15047
[11] Garcia D J *et al* 2000 *Phys. Rev. Lett.* **85** 3720
[12] Garcia D J *et al* 2002 *Phys. Rev.* B **65** 134444
[13] Koshibae W, Yamanaka M, Oshikawa M and Maekawa S 1999 *Phys. Rev. Lett.* **82** 2119
[14] Aliaga H *et al* 2001 *Phys. Rev.* B **64** 024422
[15] Yunoki S *et al* 1998 *Phys. Rev. Lett.* **80** 845
[16] Dagotto E *et al* 1998 *Phys. Rev.* B **58** 6414
[17] Neuber D R *et al* 2006 *Phys. Rev.* B **73** 014401
[18] Vallejo E, López-Urías F, Navarro O and Avignon M 2008 *J. Magn. Magn. Mater.* **320** e425

[19] Vallejo E, López-Urías F, Navarro O and Avignon M 2008 *Solid State Commun.* at press doi:10.1016/j.ssc.2008.11.001
[20] Su W P, Schrieffer J R and Heeger A J 1979 *Phys. Rev. Lett.* **42** 1698
[21] Su W P, Schrieffer J R and Heeger A J 1980 *Phys. Rev.* B **22** 2099
[22] Kagoshima S, Nagasawa H and Sambongi T 1988 *One-Dimensional Conductors* (New York: Springer)
[23] Vallejo E and Avignon M 2006 *Phys. Rev. Lett.* **97** 217203
[24] Vallejo E and Avignon M 2007 *Rev. Mex. Fís.* S **53** 1
[25] Vallejo E and Avignon M 2007 *J. Magn. Magn. Mater.* **310** 1130
[26] Mir M *et al* 2001 *Phys. Rev. Lett.* **87** 147201
[27] Mir M, Janczak J and Mascarenhas Y P 1996 *J. Appl. Crystallogr.* **39** 1356
[28] Röder H, Zang Jun and Bishop A R 1998 *Phys. Rev. Lett.* **76** 5604
[29] Fuhr J D, Avignon M and Alascio B 2008 *Phys. Rev. Lett.* **100** 216402
[30] Müller-Hartmann E and Dagotto E 1996 *Phys. Rev.* B **54** R6819
[31] Sutton A P 1993 *Electron Structure of Metals* (Oxford: Clarendon)
[32] Yamanaka M, Koshibae W and Maekawa S 1998 *Phys. Rev. Lett.* **81** 5604
[33] Yunoki S and Moreo A 1998 *Phys. Rev.* B **58** 6403
[34] Koller W *et al* 2003 *Phys. Rev.* B **67** 174418
[35] Vallejo E *J. Magn. Magn. Mater.* at press doi:10.1016/j.jmmm.2008.10.005
[36] Vallejo E 2008 *Microelectron. J.* **39** 1266